nature communications

Article

https://doi.org/10.1038/s41467-025-62092-3

Asymmetric synthesis of β-amino acid derivatives by stereocontrolled C(sp^3)-C(sp^2) cross-electrophile coupling via radical 1,2-nitrogen migration

Received: 18 November 2024

Accepted: 10 July 2025

Published online: 05 August 2025

Check for updates

Zicheng Liao[1,4], Zijun Li[1,4], Meiqiu Xiao[1,4], Youlin Deng[1,4], Zehan Ma[2], Lijuan Zhou[1], Gangliang Dai[1], Xinyu Li[1], Shuowen Wang[1], Shilu Chen[2] ✉, Jinheng Li[3] ✉ & Shi Tang[1] ✉

Optically pure non-natural β-amino acids are noteworthy molecular motifs of numerous pharmaceutically important molecules. Skeletal editing of abundant α-amino acid scaffolds via tandem radical 1,2-N-shift/cross-coupling represents a powerful tool to straightforward assemble new β-amino acid molecules; however, this strategy presents substantial challenges owing to difficulties in reactivity and regio-/enantiocontrol. Herein, we report a cross-electrophile C(sp^2)-C(sp^3) coupling of β-bromo α-amino acid esters with aryl bromides via a π-system-independent 1,2-N-shift, which allows access to α-arylated β-amino acid motifs with high efficiency and regioselectivity. Furthermore, upon the cooperative catalysis of the Ni(II)/ cyclo-Box complex and chiral phosphoric acid, this migratory coupling further achieves high enantioselectivity control in C(sp^3)–C(sp^2) bond construction. In addition, detailed experimental studies and DFT calculations have been conducted to gain insight into the mechanism and origin of the enantioselectivity. Overall, this synergistic strategy expands these methods to the challenging enantioselective C(sp^2)–C(sp^3) cross-electrophile coupling via π-system-independent radical 1,2-amino migration.

Cross-electrophile coupling is a significant complement to the classic cross-coupling reactions, in which two structurally diverse and bench-stable electrophiles can be coupled directly in the presence of an external reductant[1–7]. This strategy bypasses the preparation and handling of organometallic reagents with limited stability and commercial availability and is a sought-after technology for synthetic practitioners. In general, C–C bond formation in the cross-electrophile coupling reactions commonly occurs at a specific activated site (e.g., Cl, Br, I, etc.) preinstalled on the two coupling partners[8–14]. Accordingly, a complementary method capable of new C(sp^2)–C(sp^3) bond construction at remote, unfunctionalized sites in readily available feedstocks, which will allow straightforward access to scaffolds that would otherwise be difficult to prepare, is still in high demand for synthetic chemists. More recently, migratory cross-coupling enabled by "NiH-chain-walking" with 1,*n*-hydrogen-atom shift has emerged as the most studied method to address this challenging issue (Fig. 1a)[15–19]. Mechanistically, a two-electron β-hydride elimination/migratory insertion occurs, thus accomplishing the migration of nickel species

[1]College of Chemistry and Chemical Engineering, Jishou University, Jishou, China. [2]School of Chemistry and Chemical Engineering, Beijing Institute of Technology, Beijing, China. [3]State Key Laboratory Base of Eco-Chemical Engineering, College of Chemical Engineering, Qingdao University of Science and Technology, Qingdao, China. [4]These authors contributed equally: Zicheng Liao, Zijun Li, Meiqiu Xiao, Youlin Deng. ✉e-mail: shlchen@bit.edu.cn; jhli@hnu.edu.cn; stang@jsu.edu.cn

https://doi.org/10.1038/s41467-025-62092-3

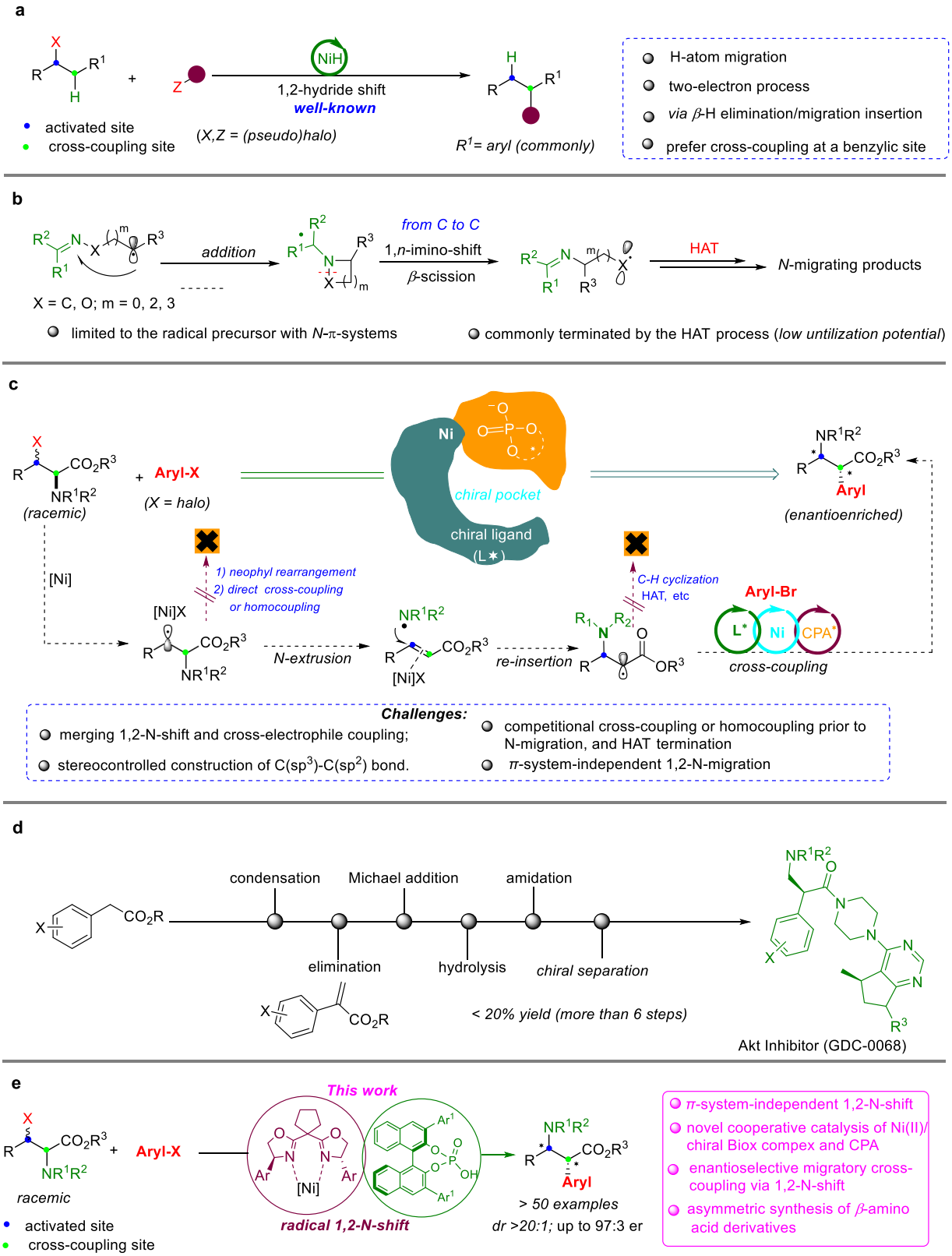

Fig. 1 | Reaction design for asymmetric migratory cross-electrophile coupling by radical π-system-independent 1,2-N-shift. a Typical migratory cross-coupling enabled by "NiH-chain walking" (previous studies). **b** Typical 1,*n*-Imino radical shift (Frey-1990, Han-2021). **c** Our design: Migratory cross-coupling with Ni/CPA cooperative catalysis. **d** Previous studies to access optimally pure bioactive β-amino acid motifs (*For example*). **e** Enantioselective migratory cross-electrophile coupling via 1,2-N-shit (*This work*).

from a preactivated to a cross-coupling site (finally to a benzylic site)[20–22]. Despite significant progress in this regard, stereocontrolled migratory coupling between two halide-based electrophiles remains a challenge[23].

Heteroatom migration/rearrangement is one of the most potent technologies for innovating new reactions and increasing molecular complexity in organic and pharmaceutical synthesis[24–28]. Over the past decade, new synthetic methods that comprise radial heteroatom migration involving the 1,*n*-shift of B-[29–32], Si-[33–35], P-[36], and halo groups[37], have been intensively exploited, delivering rapid access to heteroatom molecular scaffolds that could be in high demand by synthetic chemists. Nitrogen-based functionalities play vital roles as bioelements in bioorganic and organic chemistry. For example, the migration of radical N-functionalities occurs naturally in the lysine 1,2-aminomutase-catalyzed interconversion of L-*α*-lysine into L-*β*-lysine in *Costridia*[38]. Although N-rearrangement reactions also show high utilization prospects for organic and pharmaceutical chemistry[39–41], radical-mediated migration of N-centered functionalities remains underdeveloped. To the best of our knowledge, migratory cross-electrophile coupling enabled by a formal 1,2-N-shift has also not been reported to date. Several challenging issues must be addressed in this scenario: (a) The methods are limited to a specific radical precursor that furnishes a nitrogen-based *π*-system (e.g., imine, azide)[42–45], wherein a mechanism pattern that comprises a radical *ipso*-addition to an imino/azide *π*-bond to form an unstable, strained aziridinyl radical is commonly involved, thereby enabling a *β*-fragmentation toward formal 1,2-amino migration (Fig. 1b). Therefore, abundant and readily available organic amines without N-*π*-systems commonly display less reactivity in these documented N-migration reactions; (b) To our knowledge, however, migratory cross-electrophile coupling by a π-system-independent 1,*n*-N-shift, between two halide-based electrophiles, has never been exploited. Admittedly, several challenges remain to be addressed. First, the radical 1,2-N-shift process is readily disturbed by neophyl-type rearrangement[46], hydrogen atom transfer (HAT) or single-electron-transfer (SET) oxidation[39], instead of funnelling into a subsequent cross-coupling catalytic cycle. Secondly, the competition of intramolecular C-H cyclization[47], direct cross-coupling and homocoupling at the preactivated sites prior to amino migration exist commonly (i.e., lacking regioselectivity); (c) Thirdly, nickel-catalyzed C(sp^2)-C(sp^3) cross-coupling via radical heteroatom migration has always led to stereoablation[48,49], let alone this version of migratory coupling onto an *α*-position of an ester group which easily gives rise to racemization under basic conditions because of the newly formed stereogenic center[50–52]. Therefore, enantioselective control of migratory coupling (especial at a *α*-position of an ester group) via radical 1,2-N-shift remains a challenge. Encouraged by our recent progress in radical nitrogen migration cascades, we speculated that the nascent C(sp^3)-centered radical arising from the 1,2-N-shift of a *β*-bromo α-amino acid ester, by the judicious design of Ni/L catalytic systems, could funnel into a subsequent cross-coupling catalytic cycle with aryl halides. Furthermore, in view of these significant advances in asymmetric metal catalysis combined with organocatalysis[53–56], dual catalysis combining a Ni(II)/chiral ligand complex and chiral Brønsted acid could dictate the enantioselectivity of this migratory C(sp^2)-C(sp^3) cross-coupling and produce diverse enantioenriched β-amino acid derivatives (Fig. 1c).

Enantioenriched non-natural *β*-amino acids and analogues serve as important building blocks for bioactive scaffolds, which exist in many medicinal molecules, such as Taxol, pan-Akt inhibitors, and Jasplakinolide[57,58]. Therefore, the development of an efficient and enantioselective synthetic technique for β-amino acid derivatives has attracted much interest from organic and medicinal chemists[59–61]. Despite previous studies, there remains much to explore. Firstly, radical migration strategies enabling the catalytic enantio- and regioselective synthesis of *β*-amino acid derivatives remains underexplored[62–64]; furthermore, multiple synthetic steps and problematic chiral separation by preparative high-performance liquid chromatography (HLPC) is commonly required for this target (Fig. 1d)[65]. Secondly, although skeletal editing of abundant and easily accessible α-amino acids via a radical 1,2-N-shift sequence represents a promising approach to enantioenriched *α*-arylated *β*-amino acid esters, the method has never been successful. Given our ongoing interest in migratory coupling[66,67], we aimed to highlight the instance of migratory cross-electrophile coupling via radical 1,2-amino migration, which can be used to access *β*-amino acid motifs. Moreover, upon cooperative catalysis of the Ni(II) catalyst/ chiral bisoxazoline (Box) complex and chiral phosphoric acid (CPA), this tandem radical sequence accomplished enantioselective control of C(sp^3)-C(sp^2) cross-coupling (Fig. 1e). Inspired by Gong's pioneering work[68], the readily available and safe diboron reagent was employed as the reducing agent in our reductive coupling system. Taken together, this strategy exhibits high enantio-/diastereo-/regio-selectivity and extensive substrate compatibility, and operates avoiding use of stoichiometric quantities of unsafe metal reductants (e.g., Zn, Mn powders), toxic radical initiators, and/or elevated temperatures, thus allowing for a late-stage synthesis of non-natural *β*-amino acids and analogues.

Results

Reaction development

We initially investigated the optimal conditions for the cascade 1,2-nitrogen migration/cross-coupling reaction using the serine-derived bromide (**1**) and 4-bromobenzonitrile (**2**) as model racemic substrates (Table 1). After extensive investigation of the reaction parameters (see the 'Optimization of reaction conditions' section in Supplementary information for details), we discovered that the N-migratory coupling product (**3**) could be obtained in 74% yield when $NiBr_2$•dme (10 mol%), 2-(4,5-dihydro-1*H*-imidazol-2-yl)−4-methylpyridine **L1** (12 mol%), and B_2neo_2 (2 equiv.) were used as catalyst, ligand, and reductant, respectively. By contrast, almost no regioselective isomer (**3′**), that can be formed via direct coupling of the two pre-halogenated sites, was detected by gas chromatography (GC)–MS or ^{1}H NMR. Moreover, the relative configuration of the as-obtained product (**3**) was unambiguously confirmed by X-ray crystallography (CCDC 2383157 (for **3**), CCDC 2383157 (for **6**) and CCDC 2383157 (for **23**) contain the supplementary crystallographic data for this paper. These data are provided free of charge by the joint Cambridge Crystallographic Data Centre and Fachinformationszentrum Karlsruhe Access Structures service). The steric effect of the aromatic rings, which occur as a paired group on the N atom, contributes to suppressing the alternative intramolecular C-H cyclization toward tetrahydroisoquinoline-4-carboxylates. Accordingly, serine-derived bromides with a pair of 2,6-disubstituted benzyl groups on the N atom were designed as electrophilic coupling partners. Notably, organic diboron served as the reductant appeared to be crucial for promoting the 1,2-N-shift because using stoichiometric Zn or Mn as the reductant led to 1,4-aryl migration to afford the Smiles-type rearrangement isomer **3′** (entries 1–3). In addition, B_2neo_2 displayed the highest efficiency among the diboron reductants, including B_2pin_2 and $B_2(cat)_2$ (entries 4–5)[68–70]. Other pyridine-imidazoline ligands, such as ligands **L2**–**L3**, were also evaluated, the results showed that 2-(4,5-dihydro-1*H*-imidazol-2-yl)−4-methylpyridine **L1** remained the optimal choice (entries 6–7). Notably, bipyridine ligands **L4**–**L6** exhibited unparallel efficiency in the coupling reactions (entries 8–10).

Next, we evaluated the feasibility of enantioselective migratory cross-coupling. Among the collection of chiral *N*-based ligands (mainly Box and Bilm ligands) for this enantioselective migratory coupling with *rac*-**1**, the cyclo-bridge Box framework proved to be the most promising (see Table S2 in the Supplementary Information for details). Furthermore, a five-membered cyclo-Box ligand bearing an aryl substituent exhibited much higher reactivity and enantioselectivity (entries 11–15). Further evaluation of the substituents on the cyclo-

https://doi.org/10.1038/s41467-025-62092-3

Table 1 | Optimization of reaction conditions[a]

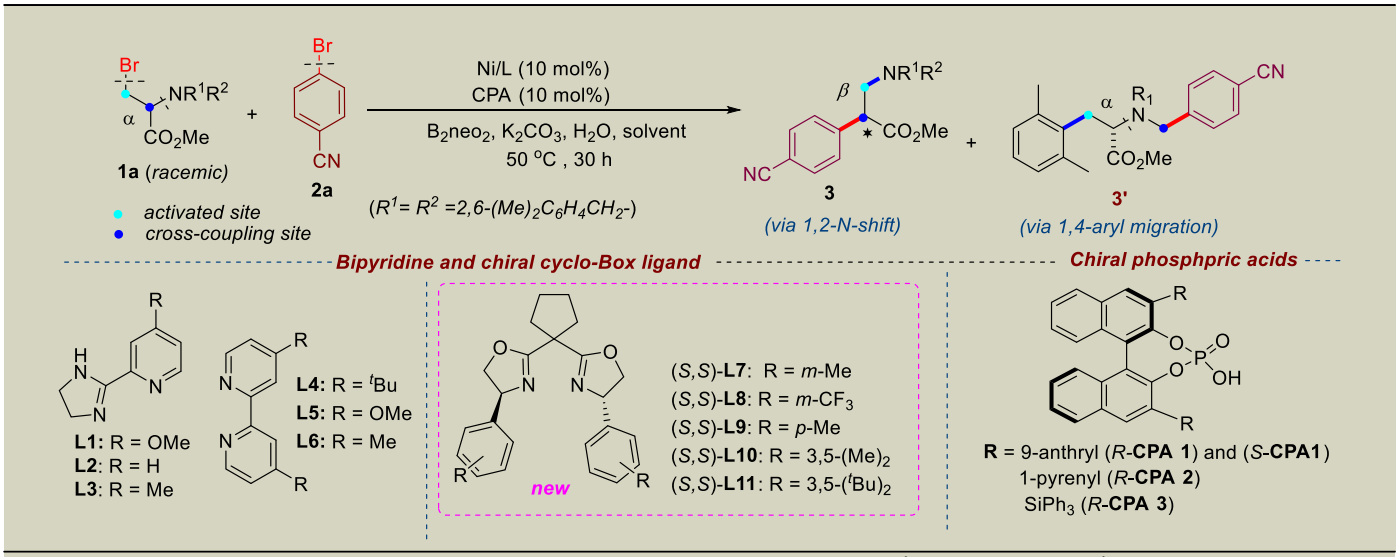

Entry	[Ni]/reductant	Ligand	CPA	Yield of 3 (%)[b]	Yield 3'(%)[b]	*er* of 3[c]
1	$NiBr_2$.dme/Zn	**L1**	–	17	61	–
2	$NiBr_2$.dme /Mn	**L1**	–	<10	21	–
3	$NiBr_2$.dme /B_2neo_2	**L1**	–	79(74)	Trace	–
4	$NiBr_2$.dme /B_2pin_2	**L1**	–	<10	Trace	–
5	$NiBr_2$.dme/B_2cat_2	**L1**	–	<10	Trace	–
6	$NiBr_2$.dme/B_2neo_2	**L2**	–	70	Trace	–
7	$NiBr_2$.dme/B_2neo_2	**L3**	–	74	Trace	–
8	$NiBr_2$.dme/B_2neo_2	**L4**	–	64	Trace	–
9	$NiBr_2$.dme/B_2neo_2	**L5**	–	61	Trace	–
10	$NiBr_2$.dme/B_2neo_2	**L6**	–	57	Trace	–
11[d]	$NiBr_2$.dme/B_2neo_2	(*S,S*)-**L7**	–	62	Trace	83:17
12[d]	$NiBr_2$.dme/B_2neo_2	(*S,S*)-**L8**	–	<10	Trace	n.d.
13[d]	$NiBr_2$.dme/B_2neo_2	(*S,S*)-**L9**	–	50	Trace	74:26
14[d]	$NiBr_2$.dme/B_2neo_2	(*S,S*)-**L10**	–	64	Trace	85:15
15[d]	$NiBr_2$.dme/B_2neo_2	(*S,S*)-**L11**	–	47	Trace	81:19
16[d]	$NiBr_2$.dme/B_2neo_2	(*S,S*)-**L10**	(*R*)-**CPA 1**	62	Trace	90:10
17[d]	$NiBr_2$.dme/B_2neo_2	(*S,S*)-**L10**	(*R*)-**CPA 2**	63(60)	Trace	97:3
18[d]	$NiBr_2$.dme/B_2neo_2	(*S,S*)-**L10**	(*S*)-**CPA 1**	59	Trace	74:26
19[d]	$NiBr_2$.dme/B_2neo_2	(*S,S*)-**L10**	(*R*)-**CPA 3**	57	Trace	89:11
20[d]	$NiCl_2$.dme/B_2neo_2	(*S,S*)-**L10**	(*R*)-**CPA 2**	56	Trace	90:10

[a] Standard conditions: **1a** (0.2 mmol.), **2a** (2 euqiv.), $NiBr_2$•dme (10 mol%), Ligand (12 mol%), B_2neo_2 (2 equiv), H_2O (2 equiv) K_2CO_3 (2 equiv), and CH_3CN/EtOH (*v*: *v* = 1.8: 0.2, 0.1 M) at 50 °C under argon atmosphere for 30 h. *B_2neo_2 bis*(neopentyl glycolato)diboron, *NMP N*-methylpyrrolidone, *DMA* dimethyl acetamide, *CPA* chiral phosphoric acid, *cat* catecholato; *pin* pinacolato. *n.d.* not detected.
[b] Yields were determined by gas chromatography (GC) using *n*-dodecane as an internal standard; isolated yields are reported in parentheses.
[c] Enantiomeric ratios (e.r.) were determined using chiral HLPC.
[d] Na_2CO_3 instead of K_2CO_3, on a 0.1 mmol scale at 40 °C for 36 h.

bridge Box ligands revealed that both the electronic properties and steric hindrance had a significant impact on the reactivity and enantioselectivity. For example, the *m*-CF_3 substituted Box ligand led to an inferior yield and enantioselectivity, whereas the 2,6-dimethyl substituted cyclo-Box ligand (**L10**) furnished the desired product **3** in 64% yield with 85:15 e.r. (entries 12 and 14). Thus encouraged, we further optimized the catalytic systems by attempting a cooperative catalysis between the Ni/Box ligand complex and a chiral Brønsted acid. Gratifyingly, suitable cooperation between CPA and the chiral Box ligand in the catalytic systems could contribute to the formation of a sterically defined chiral pocket[71], which furnished **3** with higher enantioselectivity (entries 16–19). Intriguingly, cooperation between the (*S,S*)-Box ligand (**L10**) and (*R*)-**CPA 2** proved to be optimal for the enantiomeric ratio; however, an alternative combination of the (*S,S*)-Box ligand and (*S*)-CPA hampered the enantioselectivity in this migratory coupling (entry 18). Such a stereocontrolled divergence of different combinations of Box Ligand and CPA stereoisomers for the rearrangement reactions appears to be consistent with Gong's observation of cooperative catalysis by the Pd/chiral phosphoramidite ligand complex and CPA[72]. Notably, CPA could, theoretically, easily be transformed into its sodium salts under basic conditions (using Na_2CO_3), which would really function as the as a labile ligand[55,56], according to its asymmetric catalytic efficiency. In addition, replacing $NiBr_2$•dme with $NiCl_2$•dme resulted in a slight decrease in the reactivity and enantioselectivity of this model reaction (entry 20).

Substrate scope

With the optimal reaction conditions established, the scope of aryl bromides used in this migratory cross-coupling reaction was examined under racemic conditions (Fig. 2). Gratifyingly, the migratory coupling

https://doi.org/10.1038/s41467-025-62092-3

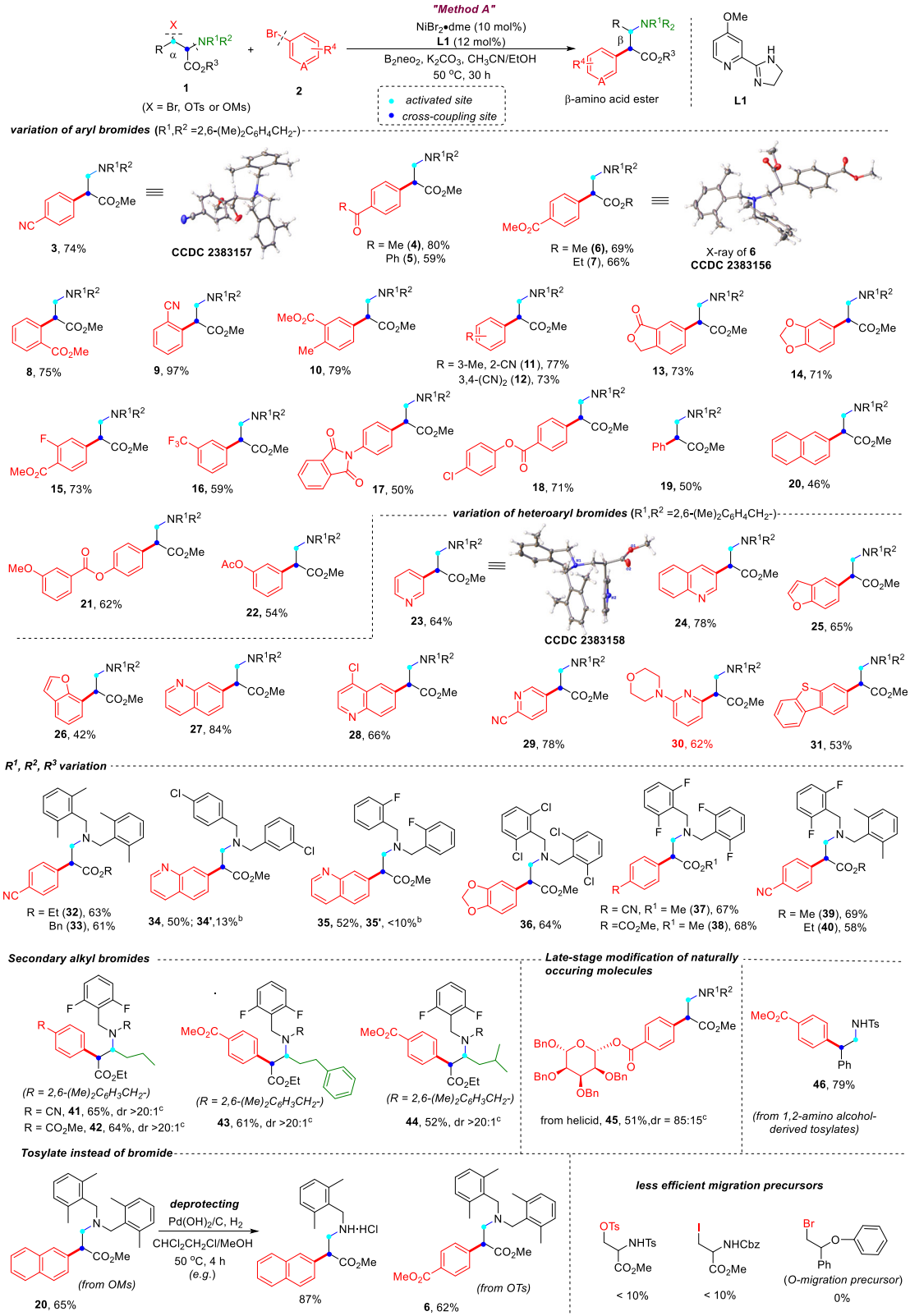

Fig. 2 | Scope of (hetero)aryl bromides and N-benzyl amino acid esters in Ni-catalyzed migratory coupling[a]. [a]Reaction conditions in "*Method A*": alkyl bromide **1** (0.2 mmol), (hetero)aryl bromide **2** (2 equiv), $NiBr_2$•dme (10 mol%), **L1** (12 mol%), B_2neo_2 (2 equiv), H_2O (2 equiv) K_2CO_3 (2 equiv) and CH_3CN/EtOH (*v: v* = 1.8: 0.2, 0.1 M) at 50 °C under argon atmosphere for 30 h; isolated yields. [b] By-products arising from intramolecular C-H cyclization. [c] Diastereoselective ratio (dr) was determined by ^1H NMR and/or ^{19}F NMR analysis.

reactions of serine-derived bromide **1a** with an array of activated aryl bromides, including 4-bromobenzonitrile, methyl 4-bromobenzoate, and 1-(4-bromophenyl)-ethenone, proceeded smoothly, leading to the formation of structurally diverse β-amino acid motifs in moderate to good yields. In addition, this set of reactions exhibited excellent regioselectivity toward the *N*-migratory coupling products (products **3**–**6**). The configuration of product **3** and **6** was unambiguously confirmed by X-ray crystallography (CCDC 2383157 (for **3**), CCDC 2383157 (for **6**) and CCDC 2383157 (for **23**) contain the supplementary crystallographic data for this paper. These data are provided free of charge by the joint Cambridge Crystallographic Data Centre and Fachinformationszentrum Karlsruhe Access Structures service). Notably, sterically hindered 2-bromobenzonitrile and methyl 2-bromobenzoate were shown to be viable coupling partners in this coupling reaction (products **8** and **9**). In addition, unactivated aryl bromides such as aniline and phenolic ester derivatives were well tolerated in this migratory reaction (products **17**–**22**). Migratory coupling also appears to be compatible with structurally diverse heteroaryl bromides and thus provides successful results for the introduction of *N*-heterocyclic motifs such as pyridine, quinoline, benzofuran, thiazole and etc., which are in high demand in medicinal chemistry (products **23**–**31**). Furthermore, the amino acid ethyl/benzyl ester was a viable precursor for the migratory coupling reaction (products **32**–**33**). Next, we evaluated the reactivity of these radical precursors with different benzyl groups tethered to the N atom and observed that diverse pairs of benzyl groups, such as *o*-F/*p*-$ClC_6H_4CH_2$, 2,6-$Cl_2C_6H_4CH_2$, 2,6-$F_2C_6H_4CH_2$, and others, were well tolerated under the optimal conditions (products **34**–**40**), albeit in moderate yield. Notably, intramolecular C-H cyclization occurs simultaneously for substrates bearing less sterically hindered benzyl groups (products **34**–**35**). In addition, we investigated the performance of α-amino acid-derived secondary bromides as the electrophiles in the coupling reactions. An array of secondary bromides was compatible with the catalytic conditions and led to structurally diverse β-amino acid esters and analogues (products **41**–**44**) in moderate yield with excellent diastereoselectivity (usually d.r. > 20:1). Furthermore, when aryl bromides derived from several bioactive molecule such as helicid, were examined, all the desired product **45** were obtained in moderate yields and with good regioselectivity. To further demonstrate the synthetic utility of this method, another type of radical coupling precursor (amino alcohol-derived tosylates) was examined as feedstock under standard conditions. As expected, the migratory cross-coupling performed well and delivered the pharmaceutically important β-arylethylamines **46**. In addition, considering the ready availability of inexpensive serine derivatives, we investigated the compatibility of serine tosylates instead of serine bromides under these reaction conditions. Delightedly, we discovered that these serine tosylates or mesylate with aryl bromides underwent sequential rearrangement and cross-coupling to afford the desired products in moderate yields. Of note, the *N*-protecting benzyl group can be removed by $Pd(OH)_2/C/H_2$ catalytic systems. Nevertheless, serine tosylate/iodine with the tosyl or CBz group on N-atom instead of a benzyl-type protecting group was less effective for migratory coupling. In addition, we further investigated the 1,2-*O*-migration reaction by employing a structurally analogous O-migratory precursor as the substrate; however, this approach did not yield the desired product.

Subsequently, we performed a preliminary evaluation of the efficiency of the newly established asymmetric catalytic systems of the Ni/chiral Box complex and CPA for the stereocontrol of migratory cross-electrophile coupling (Fig. 3). The serine-derived primary bromide **1** underwent migratory cross-coupling with structurally diverse aryl bromides in moderate yields with excellent enantioselectivity, thus resulting in stereocontrolled construction of a $C(sp^3)$-$C(sp^2)$ bond toward enantioenriched α-arylated β-amino acids (products **3, 4, 5, 6, 47, 20, 32**, and **48**). Besides, the unactivated aryl bromides was well tolerated under the asymmetric catalytic conditions (products **17, 18, 21**, and **49**). Notably, the formation of the alkyl-alkyl dimerization products, as an isomeric mixture of the homo/cross-dimerization of radicals **Int-III** and **Int-1** possibly as shown in Fig. 4, was observed to form by HRMS, as well as the homo-dimerization of aryl bromide, these existing side reactions would impress the yield of desired products to some extent, which appears to be responsible for the moderate yield outcome in many cases (usually <70% yields). Heteroaryl bromides have also proved to be compatible with asymmetric catalytic conditions, thus incorporating pharmaceutically interesting heterocyclic moieties into these amino acid skeletons, albeit with sightly decreasing enantioselectivity (products **25** and **50**). Also, a pair of benzyl group 2,6-$F_2C_6H_4CH_2$ on the N-atom, instead of 2,6-$Me_2C_6H_4CH_2$, were observed to be viable precursor for migratory coupling, thus accessing enantioenriched β-amino acid esters bearing pharmaceutically important fluorine atom (products **37, 38, 39, 40**, and **51**). In addition, the natural molecular moieties were successfully and stereospecifically installed on these amino acid scaffolds using this migratory coupling strategy (dr >20:1; product **45**). Undoubtedly, the abovementioned successes would endow this asymmetric catalysis strategy with broad utilization prospects for the synthesis of complex non-natural amino acids and analogues[24–28]. Furthermore, by using this migratory cross-coupling strategy, a *pan*-Atk inhibitor analogue can be successfully prepared in two steps with excellent enantioselectivity, avoiding multiple stepwise syntheses (especially challenging chiral separation steps), as previously reported[65,73].

Mechanistic investigations

Next, control experiments were conducted to elucidate the cascade 1,2-N-shift/cross-electrophile coupling (Fig. 4). First, the use of the radical scavenger, 2, 2, 6, 6-tetramethyl-1-piperidinyloxyl (TEMPO•) was investigated. As expected, the 1,2-N-shift process was significantly suppressed, and HRMS analysis confirmed the formation of the TEMPO–**1** adduct (**53**), suggesting the involvement of a radical-mediated process in the reaction (eq 1). In addition, a standard radical clock (cyclopropane) was subjected to the optimal reaction conditions, and none of the expected *β*-arylation of the amino acid ester **55** was observed. Instead, the formation of product **54** via a radical cyclopropane ring-opening process was observed by HRMS and ^{1}H NMR (eq 2). This clearly indicates that the alkyl radical formed via dehalogenation by Ni likely triggers a sequential migratory cross-coupling reaction[74]. Notably, crossover experiments revealed a distinct mechanistic preference: the aminyl radical re-addition to acrylate predominantly occurs through an in-cage pathway, yielding products **3** (28%) and **41** (23%). In contrast, the out-of-cage addition products **56** and **57** were obtained in significantly lower yields (<10%) (eq 3). Based on our investigation of the cascade migration/cross-coupling of β-bromo amino acid esters, we discovered that 1,2-N-shift was beneficial in the kinetically favored *N*-extrusion/1,4-addition sequence, whereas 1,3-N-shift using a γ-bromo amino acid ester as the precursor appeared to be less effective (eq 4). Radical 1,2-N-shift/Heck-type coupling cascades were also observed when using *α*-trifluoromethyl alkenes as the Michael acceptors, which also suggested that an electrophilic α-carboxyl radical via 1,2-N-shift should generate in this radical relay (eq 5). In addition, The EPR spectrum of the reaction in the presence of $NiBr_2$•dme/**L1**/K_2CO_3/B_2neo_2/**1** with the spin-trapping reagent 5,5-Dimethyl-1-pyrroline-*N*-oxide, under standard conditions, indicated that some alkyl radical species were produced along with the desired product **3**, confirming that a radical-mediated process was involved in the 1,2-N-shift process (eq 6). Furthermore, we performed a control experiment using aziridine as the radical precursor under the standard reaction conditions (eq 7). The results revealed that no corresponding product derived from a ring-opening/cross-coupling sequence was detected. This observation suggests that the radical-mediated nitrogen migration in our system may proceed via a mechanism distinct from those proposed by Doyle et al.[75]. Subsequently, the ^{11}B NMR

https://doi.org/10.1038/s41467-025-62092-3

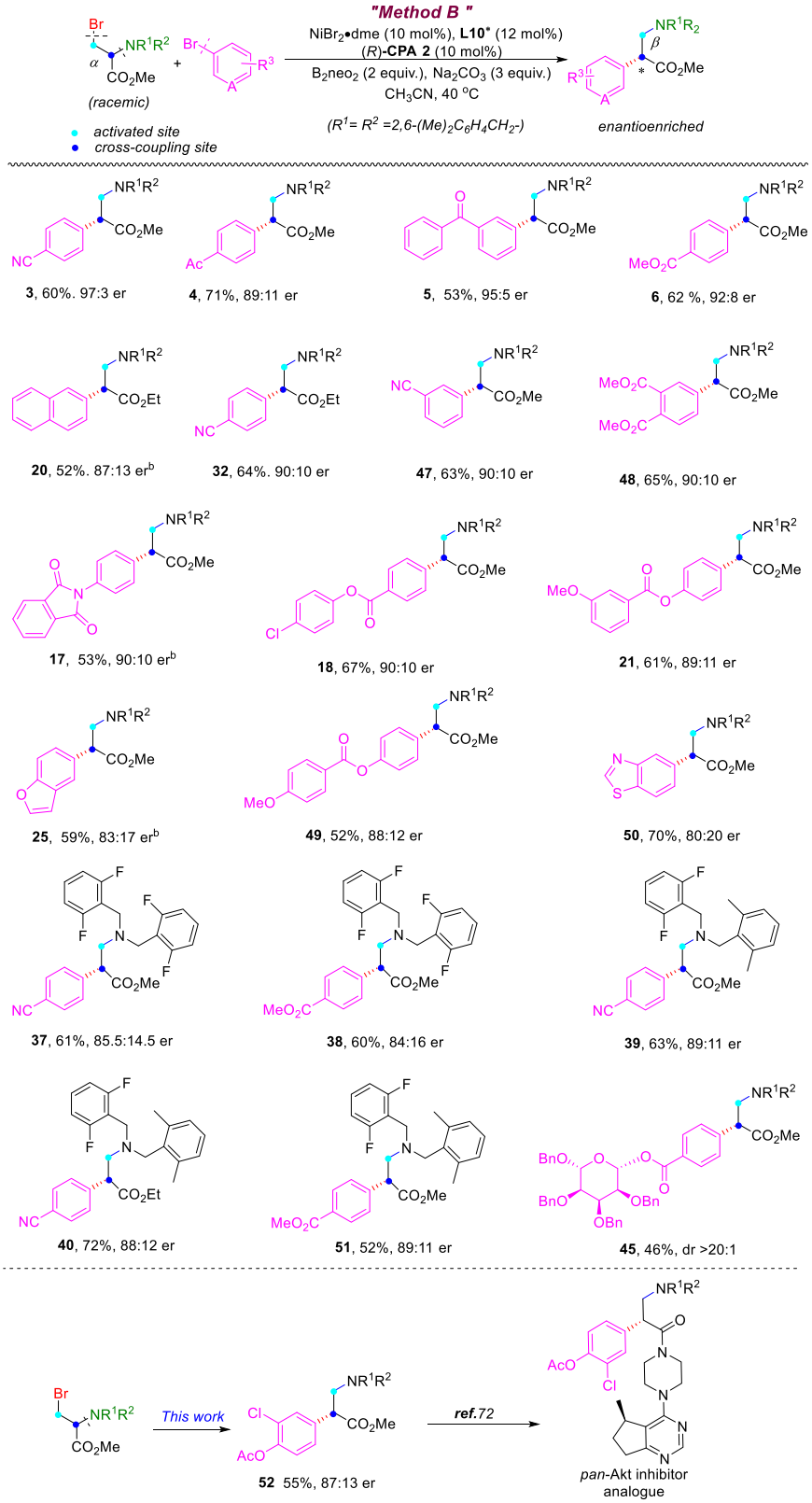

Fig. 3 | Ni/CPA-catalyzed enantioselective migratory cross-electrophile coupling by 1,2-N-shift[a]. [a]Reaction conditions in "*Method B*": alkyl bromide **1** (0.1 mmol), (hetero)aryl bromide **2** (2 equiv.), $NiBr_2$.dme (10 mol%), **L10*** (12 mol%), (*R*)-**CPA-2** (10 mol%), B_2neo_2 (2 equiv), H_2O (2 equiv) Na_2CO_3 (3 equiv) and CH_3CN (1 mL, 0.1 M) at 40 °C under argon atmosphere for 36 h; Enantiomeric ratios (e.r.) were determined using chiral HLPC; isolated yields. [b] (11b*R*)−4-Hydroxy-2,6-bis[4-(2-naphthalenyl)phenyl]−4-oxide dinaphtho[2,1-d:1′,2′-f][1,3,2]dioxaphosphepin (**CPA-7**) instead of **CPA-2**.

https://doi.org/10.1038/s41467-025-62092-3

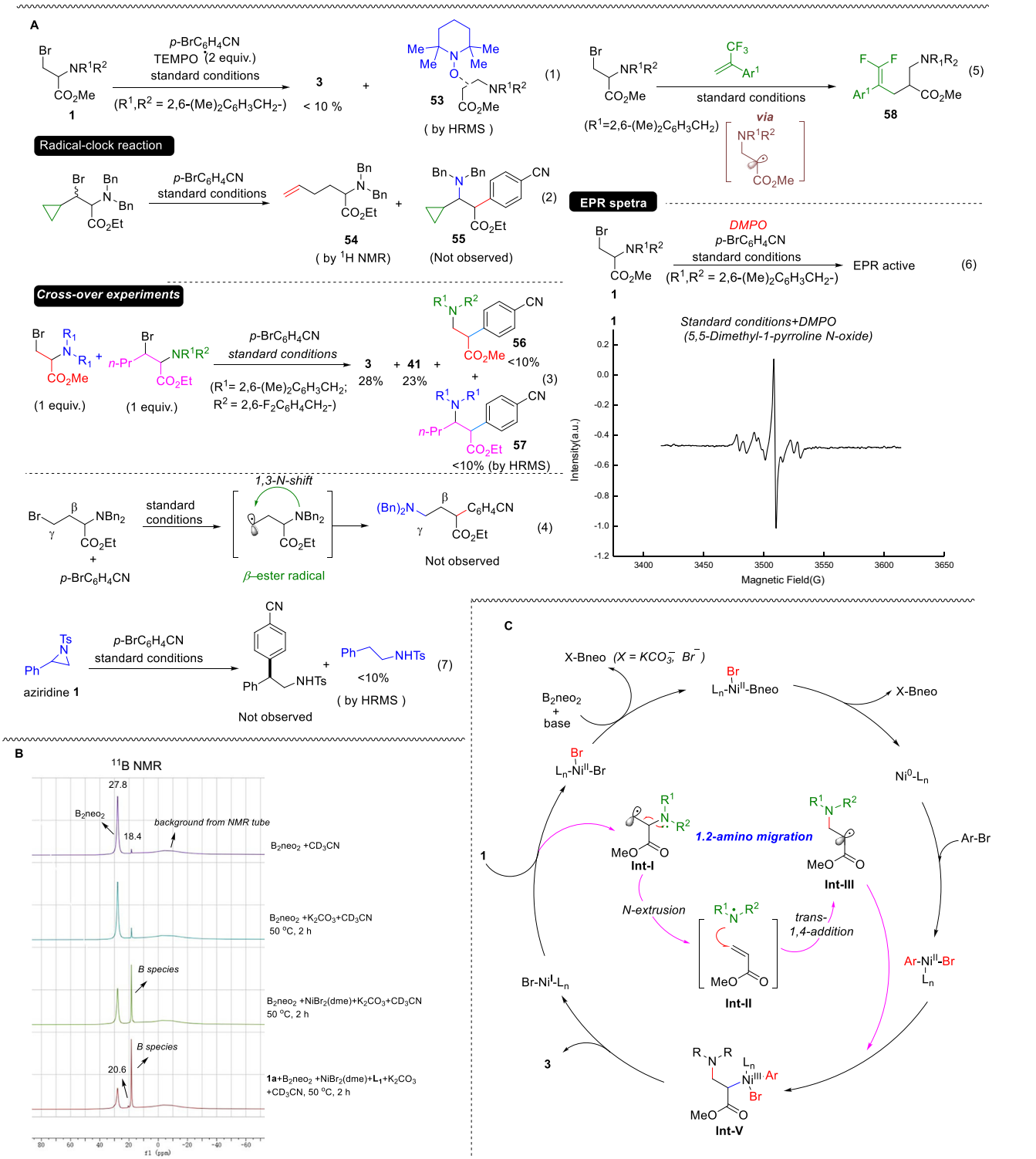

Fig. 4 | Mechanism studies on the migratory cross-electrophile coupling via radical 1,2-N-shift. A Control experiments. **B** ^{11}B NMR studies on the cleavage of B-B bond. **C** Proposed mechanism for the migratory coupling.

spectra confirmed that the Ni complex mediated the activation and cleavage of the B-B bond in B_2neo_2, thereby facilitating the generation of active Ni-Bneo species involved in the migratory coupling catalytic cycle, which aligns with a previous report (Fig. 4B)[68,70].

Based on the experimental results and previously reported mechanisms[12–78], the proposed mechanism for this cascade reaction is shown in Fig. 4C (CCDC 2383157 (for **3**), CCDC 2383157 (for **6**) and CCDC 2383157 (for **23**) contain the supplementary crystallographic data for this paper. These data are provided free of charge by the joint Cambridge Crystallographic Data Centre and Fachinformationszentrum Karlsruhe Access Structures service). First, B_2neo_2 is activated by the L_n-$Ni^{II}Br_2$ complex with the aid of a base, thereby generating both the Ni-B complex, L_n-Ni^{II}(Bneo)Br, and carboxylic or bromoboronate (X-Bneo)[68,76]. Next, L_n-Ni^{II}(Bneo)Br undergoes reductive extrusion of the Br-Bneo species to deliver the L_nNi^0 species[77–79], thus realizing the two-electron reduction of the Ni(II) to Ni(0) species in the Ni catalytic

https://doi.org/10.1038/s41467-025-62092-3

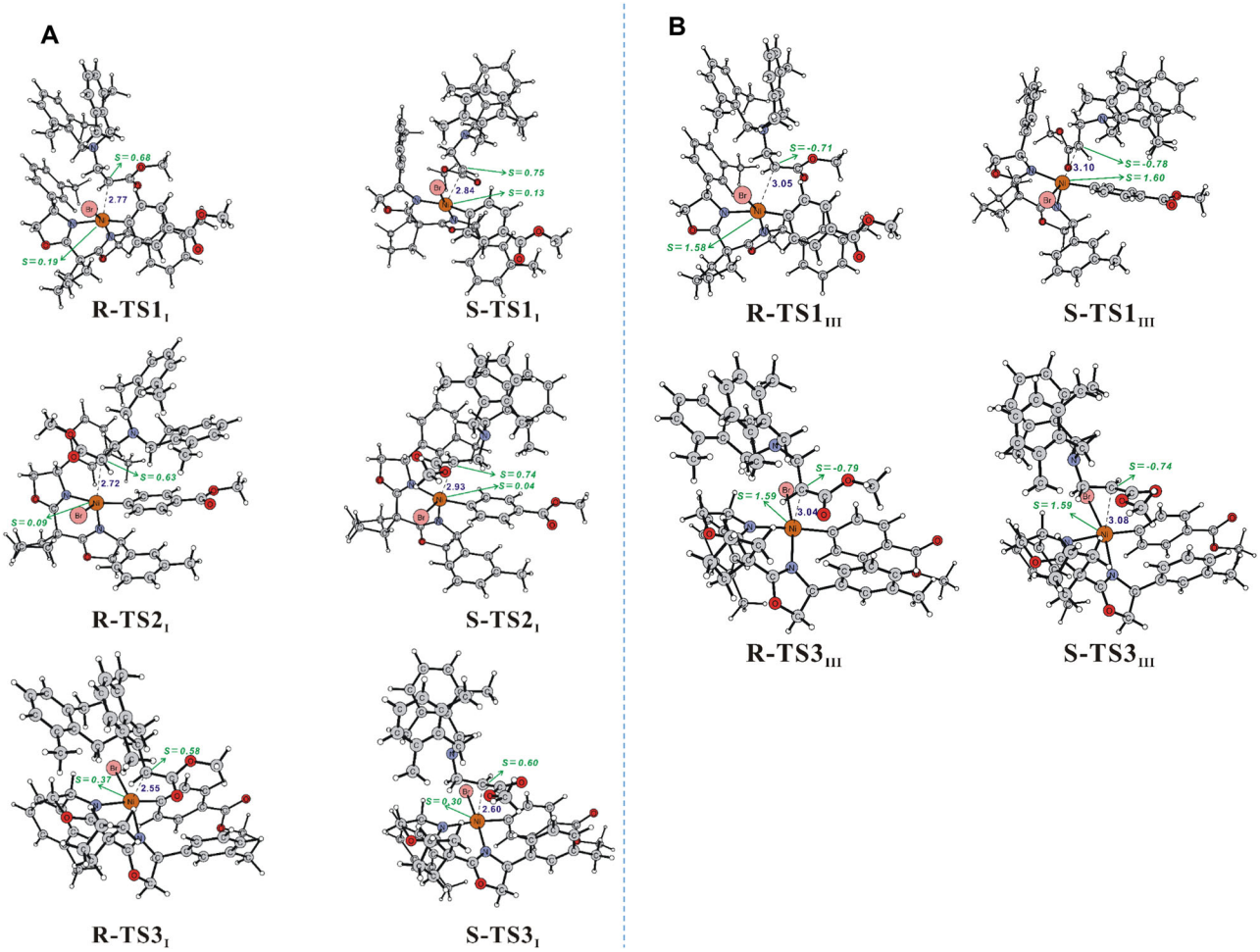

Fig. 5 | DFT optimized structures of the transition states. A Optimized structures of the transition states for the radical addition with the single-state Ni^{III} complex as the active species. **B** Triplet-state Ni^{III} complex as the active species.

Table 2 | Properties of diverse transition states for the radical addition

Multiplicity at Ni	Enantioselectivity	Conformation	Free energy barrier (kcal/mol)
Triple State[a]	*S*-	**S-TS1$_{III}$**	13.4
		S-TS2$_{III}$	5.3
		S-TS3$_{III}$	16.1
	R-	**R-TS1$_{III}$**	6.5
		R-TS2$_{III}$	4.7
		R-TS3$_{III}$	18.1
Single-state[a]	*S*-	**S-TS1$_{I}$**	8.4
		S-TS2$_{I}$	13.7
		S-TS3$_{I}$	12.9
	R-	**R-TS1$_{I}$**	7.6
		R-TS2$_{I}$	13.7
		R-TS3$_{I}$	9.0

[a] Optimized structures are displayed in Figs. 5 and 6.

cycle. By contrast, the L_n-$Ni^{I}Br$ complex undergoes a SET oxidation process with serine-derived bromide (**1**), yielding the radical intermediate **Int-I** and a Ni(II) intermediate, which then participates in the next catalytic cycle. Notably, the in situ-generated X-Bneo species could act as a Lewis acid to coordinate with the NR^1R^2 moiety in intermediate **int-I**, which would contribute to the cleavage of the C(sp^3)-N bond[80]. This mechanistic rationale provides a plausible explanation for the observed divergent migration preferences: while employing $B_2(neo)_2$ as the reductant favors radical 1,2-N-shift (as discussed in Table 1), the use of zinc powder selectively enables 1,4-aryl migration[66]. Subsequently, the NR^1R^2 species of the nascent intermediate **int-I** is extruded to form methyl acrylate (**int-II**) (In the reaction, GC-MS analysis successfully detected the formation of side-product olefin and (2,6-$Me_2C_6H_3CH_2$)NH during the N-extrusion process from the intermediate **Int-1** to **Int-2** in Fig. 4C, please see the 'Control experiments' section in Supplementary Information for details). This is followed by the 1,4-addition of the nascent $\bullet NR^1R^2$ radical (likely exhibiting nucleophilic character[81]) to the resulting methyl acrylate to yield intermediate **Int-III**, thus realizing the formal radical 1,2-amino migration (see the 'DFT Calculations' section in Supplementary information for details on this "N-extrusion/1,4-addition process). During this DFT calculations, we attempted to locate an aziridine-type radical intermediate by cyclizing on the lone electron pair of the N-atom of **Int-I**, but were unsuccessful. One likely explanation for this failure is the high ring strain associated with the three-membered ring. Thus, our DFT calculations revealed that the cyclization on the lone electron pair of the N-atom of Int-I to produce an aziridine-type radical intermediate, enabling 1,2-N-shift could not occur. Notably, *trans* addition is favored during the *re*-addition process, which is consistent with the observation that this migratory coupling typically exhibits high diastereoselectivity (*syn/trans* > 20:1). In the cross-coupling catalytic cycle, the Ni^0 species first undergoes

https://doi.org/10.1038/s41467-025-62092-3

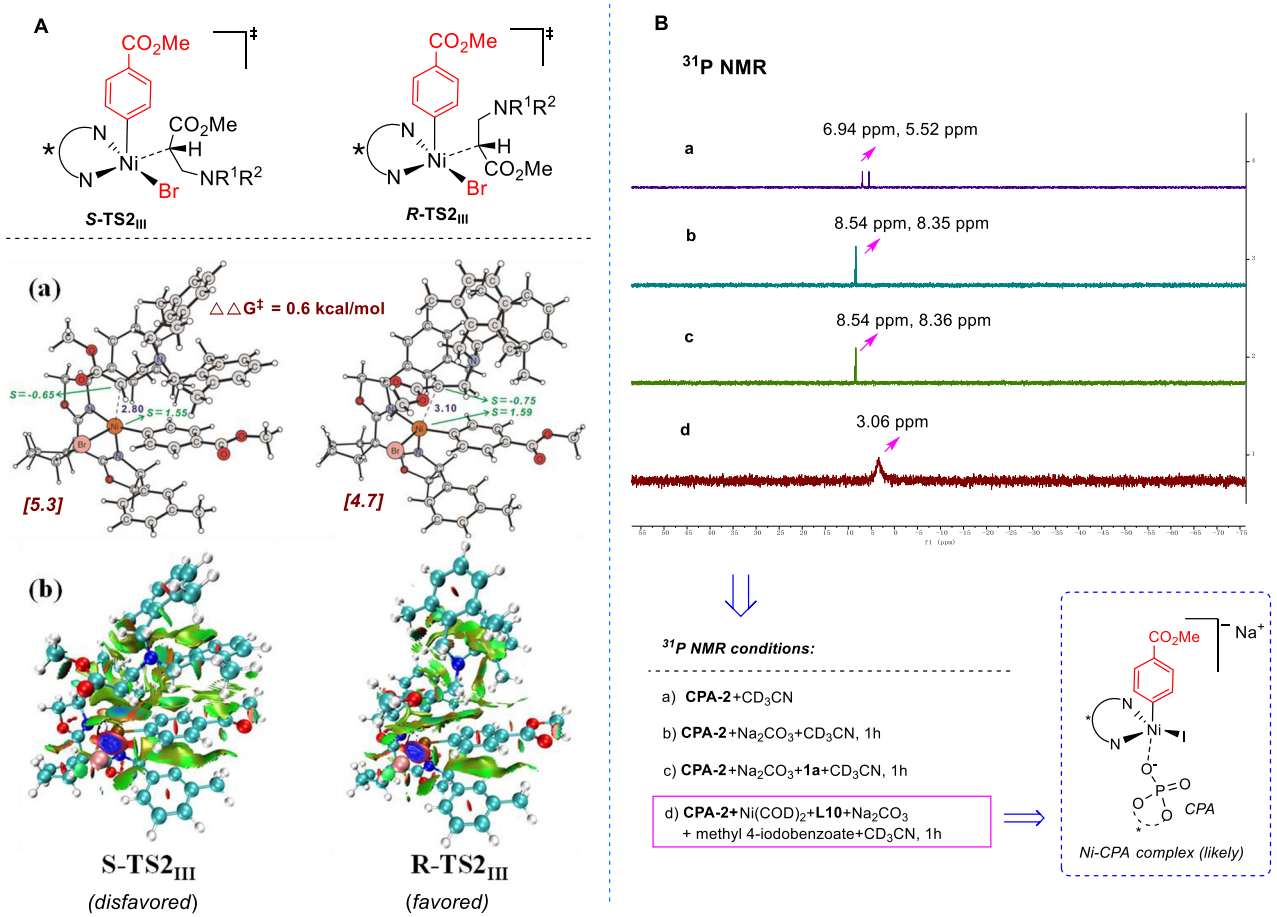

Fig. 6 | Non-covalent interaction (NCI) analysis and ^{31}P NMR studies. A DFT investigation on the origin of enantioselectivity in the radical addition step: **a** Optimized structures of the lowest-barrier transition states for the formation of *S*-intermediates (S-TS2$_{III}$) and *R*-intermediates (R-TS2$_{III}$). **b** Their non-covalent interaction (NCI) analysis. In the structures, the distances are in angstrom (Å) and the unpaired spin populations are shown with the indication of "S". In the NCI analysis, the green clouds (visualized as color-filled reduced density gradient isosurface) indicate dispersion interaction. **B** ^{31}P NMR studies on the role of CPA in the asymmetric catalytic systems.

oxidative addition to the aryl bromide to produce an ArNi^{II}(L$_n$)Br complex. Subsequently, the α-ester radical (**Int-III**) generated by the 1,2-amino migration adds to ArNi^{II}(L$_n$)Br to form a Ni^{III} complex (**Int-IV**). Finally, the Ni^{III} complex undergoes reductive elimination to furnish the desired product (**3**) and the L$_n$-Ni^{I} complex, which is directly involved in the next catalytic cycle. Notably, in the presence of water and a base, B_2neo_2 can undergo hydrolysis and liberate traces of hydrogen (see the 'Control experiments' section in Supplementary information for details)[82], which appears to reduce $NiBr_2$.dme to the Ni(I) or Ni(0) species to restart the Ni catalytic cycle.

Subsequently, our calculations also provide insight into the origins of stereocontrol in this migratory cross-coupling (Fig. 5). By using density functional theory (DFT) calculations (the computational methods are provided in the 'DFT Calculations' section in Supplementary information)[83–85], we investigated in detail the origin of enantioselectivity in the radical addition step. Notably, the calculations were operated by using the chiral ligand (*S,S*)-*m*-tolyl-Box **L7**, methyl *p*-bromobenzoate, and serine derived bromide **1** as model substrate. Given that the Ni catalyst exhibits nearly identical free energies between its triplet and singlet states (with the triplet state being slightly more stable by 1.2 kcal/mol), we examined the radical addition to both states of the Ni catalyst. Transition states for the radical addition leading to both *R*- and *S*-intermediates were optimized. For each enantioselectivity, three distinct initial conformations of the interaction between the catalyst and the radical substrate were considered, resulting in a total of twelve optimized transition states (Table 2). As shown in Table 2, the transition states of **S-TS2$_{III}$** and **R-TS2$_{III}$** exhibit the lowest free energy barriers for the formation of *S*- and *R*-intermediates, respectively, with the latter being 0.6 kcal/mol more favourable. According to the Boltzmann distribution, this barrier difference corresponds to an approximate enantiomeric ratio of 3:1 favoring the formation of the *R*-intermediate, a prediction that aligns closely with experimental observations. Moreover, structural and non-covalent interaction analysis reveals that **R-TS2$_{III}$** benefits from the reduced steric hindrance around the ester group of the radical substrate, resulting in a parallel arrangement and stronger dispersion interactions between the ester-radical conjugated system of the radical substrate and the Ni center of the catalyst. These factors are likely responsible for the observed enantioselectivity favoring the *R*-intermediate. Enlightened by Guo's study on the synergistic catalysis—combining a phosphine–nickel complex and an axially chiral sodium dicarboxylate[56], we conducted in-situ ^{31}P NMR studies to identify chiral phosphoric acid (**CPA-2**) species participating in the asymmetric catalytic cycle (Fig. 6B). Initial characterization of CPA in CD_3CN revealed two single resonances at δ = 6.94 ppm and 5.52 ppm. Subsequent neutralization with Na_2CO_3 induced complete disappearance of the CPA signal, concomitant with the emergence of a new doublet (δ = 8.35 and 8.54 ppm) corresponding to phosphate formation. Remarkably, introducing migratory precursor **1a** to the CPA/Na_2CO_3 system maintained this doublet pattern (δ = 8.36 ppm and 8.54 ppm),

suggesting no direct interaction between precursor **1a** and the phosphate intermediate. Intriguingly, further addition of $Ni(COD)_2$, **L10**, and methyl 4-iodobenzoate (in situ generating the Ar-NiL-X complex as shown in Fig. 6B) to the binary system of CPA and Na_2CO_3 resulted in the emergence of a distinct ^{31}P NMR resonance at δ = 3.06 ppm. This shift, along with other spectral changes, indicates the formation of new nickel-phosphate complexes with structural modifications including ligand coordination mode, steric reorganization, etc. These observations collectively demonstrate that (1) CPA undergoes base-mediated conversion to phosphate species under catalytic conditions, and (2) synergistic coordination between the CPA-derived phosphate and the Ni/**L10** complex generates a sterically defined chiral pocket. To further elucidate the enantioselectivity enhancement induced by CPA, we conducted additional DFT calculations on the CPA-mediated radical addition step. Analysis of the CPA-containing catalytic system showed that transition states $\mathbf{R\text{-}TS2_{III.P}}$ and $\mathbf{S\text{-}TS2_{III.P}}$ have the lowest free energy barriers for forming the *S*- and *R*-intermediates, respectively. $\mathbf{R\text{-}TS2_{III.P}}$ is 1.8 kcal/mol more stable than $\mathbf{S\text{-}TS2_{III.P}}$ (see 'DFT Calculations' section in Supplementary information for details). According to the Boltzmann distribution, this barrier difference corresponds to an approximate enantiomeric ratio of ~18:1 (*R*: *S*), a prediction that aligns with experimental observations. These ^{31}P NMR and DFT results demonstrate that the synergistic effects between CPA phosphate and nickel/Box catalysis enable enantioselective control over the radical cascade, which involves a 1,2-N-shift and $C(sp^3)$-$C(sp^2)$ cross-electrophile coupling.

Discussion

In summary, we have disclosed a nickel/CPA co-catalyzed enantio- and regioselective migratory cross-electrophile coupling by π-system-independent 1,2-N-shift, allowing the straightforward synthesis of the non-natural α-arylated *β*-amino acid motifs through skeletal editing of β-bromo α-amino acid esters with aryl bromides in excellent high regio- and enantioselectivity. Upon cooperative catalysis of a nickel/chiral cyclo-Box complex and CPA, the radical cascades further realized enantioselective building of a $C(sp^2)$-$C(sp^3)$ bond, thus accomplishing skeletal editing of racemic β-bromo α-amino acid esters toward enantioenriched β-amino acids. Notably, this success expands these strategies toward the challenging enantioselective migratory $C(sp^2)$–$C(sp^3)$ cross-coupling at the alpha position of the ester moiety. In addition, the origin of the enantioselectivity in the radical addition step was clarified by DFT calculations. The radical relay is catalyzed by an asymmetric combination of a chiral cyclo-Box ligand and CPA, using organic diboron as a safe reductant and exhibits a broad scope and excellent enantio- and regioselectivity. The reaction is a powerful platform for the asymmetric synthesis of *β*-amino acid motifs from abundant and easily accessible α-amino acids.

Methods

Typical experimental procedure for migratory cross-coupling of β-bromo α-amino acid esters with aryl bromides

Method A. To a 10 mL Schlenk tube with screw-cap was added β-bromo α-amino acid ester (0.2 mmol, if solid), aryl bromide/tosylate (2 equiv, if solid), $NiBr_2$(dme) (10 mol%), (12 mol%), **L1** (12 mol%), K_2CO_3 (2 equiv), B_2neo_2 (2 equiv). The tube was evacuated and back-filled with argon (this process was repeated three times), CH_3CN/EtOH (*v*:*v* = 1.8:0.2) were added consecutively via syringe with β-bromo α-amino acid ester (0.2 mmol, if liquid) and aryl bromide/toyslate (0.4 mmol, if liquid). The resulting mixture was bubbled with argon to degas for 1 min and stirred at 50 °C for 30 h. **Note: a stirring speed above 800 rpm is highly important for reproducibility**. The resulted mixture was filtered through a short plug of silica gel to remove metal salts, and diluted with Et_2O (50 mL). The filtrate was poured into a separatory funnel and partitioned with brine (20 mL). The aqueous layer was then extracted with diethyl ether (3 × 20 mL). The organic layer was dried over anhydrous Na_2SO_4 and concentrated in vacuo. The residue was purified by flash chromatography on silica gel (eluent: *n-hexane/ethyl acetate*) to afford the corresponding products (**3**–**46**) in a yield as listed in Fig. 2.

Method B (Asymmetric). To 3 mL vial were added sequentially $NiBr_2$(dme) (10 mol%), (*S,S*)-**L10*** (12 mol%), (*R*)-**CPA*-2** (10 mol%), β-bromo α-amino acid ester (0.1 mmol), aryl bromide (2 equiv), Na_2CO_3 (3 equiv), B_2neo_2 (2 equiv), and CH_3CN (0.5 mL) in a dry glovebox. The vial was closed with a screw cap containing a PTFE septum, taken outside the dry box, and the solution of CH_3CN (0.5 mL) with H_2O (2.0 equiv.) were added consecutively via syringe under a positive flow of argon. The resulting mixture was stirred at 40 °C for 36 h. **Note: a stirring speed above 800 rpm is highly important for reproducibility**. The resulted mixture was filtered through a short plug of silica gel to remove metal salts, and diluted with Et_2O (30 mL). The filtrate was poured into a separatory funnel and partitioned with brine (10 mL). The aqueous layer was then extracted with diethyl ether (3 × 20 mL). The organic layer was dried over anhydrous Na_2SO_4 and concentrated in vacuo. The residue was purified by flash chromatography on silica gel (eluent: n-hexane/ethyl acetate) to afford the corresponding enantioenriched β-amino acid esters in a yield as listed in Fig. 3.

Data availability

The data supporting the findings of this study are available with the article and its Supplementary Information. Crystallographic data for the structures reported in this Article have been deposited at the Cambridge Crystallographic Data Centre, under deposition numbers CCDC 2383156 (**6**), CCDC 2383157 (**3**), and CCDC 2383158 (**23**). Copies of the data can be obtained free of charge via https://www.ccdc.cam.ac.uk/structures/. All data are available from the corresponding author upon request. Source data are provided with this paper.

References

1. Weix, D. J. Methods and mechanisms for cross-electrophile coupling of Csp^2 halides with alkyl electrophiles. *Acc. Chem. Res.* **48**, 1767–1775 (2015).
2. Everson, D. A. & Weix, D. J. Cross-electrophile coupling: principles of reactivity and selectivity. *J. Org. Chem.* **79**, 4793–4798 (2014).
3. Liu, J.-D., Ye, Y., Jonathan, L. S. & Gong, H.-G. Cross-electrophile couplings of activated and sterically hindered halides and alcohol derivatives. *Acc. Chem. Res.* **53**, 1833–1845 (2020).
4. Knappke, C. E. I. et al. Reductive cross-coupling reactions between two electrophiles. *Chem. Eur. J.* **20**, 6828–6842 (2014).
5. Moragas, T., Correa, A. & Martin, R. Metal-catalyzed reductive coupling reactions of organic halides with carbonyl-type compounds. *Chem. Eur. J.* **20**, 8242–82589 (2014).
6. Wang, X., Dai, Y.-J. & Gong, H.-G. Nickel-catalyzed reductive couplings. *Top. Curr. Chem.* **374**, 43 (2016).
7. Pang, X.-B., Su, P.-F. & Shu, X.-Z. Reductive cross-coupling of unreactive electrophiles. *Acc. Chem. Res.* **55**, 2491–2509 (2022).
8. Everson, D. A., Shrestha, R. & Weix, D. J. Nickel-catalyzed reductive cross-coupling of aryl halides with alkyl halides. *J. Am. Chem. Soc.* **132**, 920–921 (2010).
9. Zhang, P., Le, C. & MacMillan, D. W. C. Silyl radical activation of alkyl halides in metallaphotoredox catalysis: a unique pathway for cross-electrophile coupling. *J. Am. Chem. Soc.* **138**, 8084–8087 (2016).
10. Duan, J.-C., Du, Y.-F., Pang, X.-B. & Shu, X.-Z. Ni-catalyzed cross-electrophile coupling between vinyl/aryl and alkyl sulfonates: synthesis of cycloalkenes and modification of peptides. *Chem. Sci.* **10**, 8706–8712 (2019).

11. Wang, J.-W., Zhao, J.-H. & Gong, H.-G. Nickel-catalyzed methylation of aryl halides/tosylates with methyl tosylate. *Chem. Commun.* **53**, 10180–10183 (2017).
12. Hansen, E. C. et al. New ligands for nickel catalysis from diverse pharmaceutical heterocycle libraries. *Nat. Chem.* **8**, 1126–1130 (2016).
13. Li, X., Feng, Z., Jiang, Z.-X. & Zhang, X. Nickel-catalyzed reductive cross-coupling of (hetero) aryl iodides with fluorinated secondary alkyl bromides. *Org. Lett.* **17**, 5570–5573 (2015).
14. Kadunce, N. T. & Reisman, S. E. Nickel-catalyzed asymmetric reductive cross-coupling between heteroaryl iodides and α-chloronitriles. *J. Am. Chem. Soc.* **137**, 10480–10483 (2015).
15. Fiorito, D., Scaring, S. & Mazet, C. Transition metal-catalyzed alkene isomerization as an enabling technology in tandem, sequential and domino processes. *Chem. Soc. Rev.* **50**, 1391–1406 (2021).
16. Sommer, H., Hernandez, F. J., Martin, R. & Marek, L. Walking metals for remote functionalization. *Acs. Cent. Sci.* **4**, 153–165 (2018).
17. Hernandez, F. J., Moragas, T., Cornella, J. & Martin, R. Remote carboxylation of halogenated aliphatic hydrocarbons with carbon dioxide. *Nature* **545**, 84–88 (2017).
18. Li, Y.-Y. & Yin, G.-Y. Nickel chain-walking catalysis: a journey to migratory carboboration of alkenes. *Acc. Chem. Res.* **56**, 3246–3259 (2023).
19. Vasseur, A., Bruffaerts, J. & Marek, L. Remote functionalization through alkene isomerization. *Nat. Chem.* **8**, 209–219 (2016).
20. Kumar, G. S. et al. Nickel-catalyzed chain-walking cross-electrophile coupling of alkyl and aryl halides and olefin hydroarylation enabled by electrochemical reduction. *Angew. Chem. Int. Ed.* **59**, 6513–6519 (2020).
21. He, Y.-L. et al. Regio-and enantioselective remote hydroarylation using a ligand-relay strategy. *Nat. Commun.* **13**, 2471 (2022).
22. Wang, W. et al. Migratory arylboration of unactivated alkenes enabled by nickel catalysis. *Angew. Chem. Int. Ed.* **58**, 4612–4616 (2019).
23. Chen, F.-L. et al. Remote migratory cross-electrophile coupling and olefin hydroarylation reactions enabled by in situ generation of NiH. *J. Am. Chem. Soc.* **139**, 13929–13935 (2017).
24. Wu, X.-X. & Zhu, C. Radical-mediated remote functional group migration. *Acc. Chem. Res.* **53**, 1620–1636 (2020).
25. Chen, Z.-M., Zhang, X.-M. & Tu, Y.-Q. Radical aryl migration reactions and synthetic applications. *Chem. Soc. Rev.* **44**, 5220–5245 (2015).
26. Chen, Y.-L., Chang, L. & Zuo, Z.-W. Visible light photoredox-induced Smiles rearrangement. *Acta Chim. Sin.* **77**, 794–802 (2019).
27. Allart-Simon, I., Gerard, S. & Sapii, J. Radical Smiles rearrangement: an update. *Molecules* **21**, 878 (2016).
28. Wu, X.-X., Ma, Z.-G., Feng, T.-T. & Zhu, C. Radical-mediated rearrangements: past, present, and future. *Chem. Soc. Rev.* **50**, 11577–11613 (2021).
29. Jana, K., Bhunia, A. & Studer, A. Radical 1,3-difunctionalization of allylboronic esters with concomitant 1,2-boron shift. *Chem* **6**, 512–522 (2020).
30. Wang, D.-H., Muck-Lichtenfeld, C. & Studer, A. 1,*n*-bisborylalkanes via radical boron migration. *J. Am. Chem. Soc.* **142**, 9119–9123 (2020).
31. Zhao, B.-L. et al. An olefinic 1,2-boryl-migration enabled by radical addition: construction of *gem*-Bis(boryl)alkanes. *Angew. Chem. Int. Ed.* **58**, 9448–9452 (2019).
32. Ge, J.-F. et al. Ir-catalyzed enantioselective synthesis of *gem*-diborylalkenes enabled by 1,2-boron shift. *Angew. Chem. Int. Ed.* **62**, e202307447 (2023).
33. Brook, A. G. Isomerism of Some α-Hydroxysilanes to Silyl Ethers. *J. Am. Chem. Soc.* **80**, 1886–1889 (1958).
34. Deng, Y.-F., Liu, Q. & Smith, A. B. Oxidative [1,2]-brook rearrangements exploiting single-electron transfer: photoredox-catalyzed alkylations and arylations. *J. Am. Chem. Soc.* **139**, 9487–9490 (2017).
35. Laskar, R. et al. γ-amino alcohols via energy transfer enabled Brook rearrangement. *J. Am. Chem. Soc.* **146**, 10899–10907 (2024).
36. Xie, D.-T. et al. Regioselective fluoroalkylphosphorylation of unactivated alkenes by radical-mediated alkoxyphosphine rearrangement. *Angew. Chem. Int. Ed.* **61**, e202203398 (2022).
37. Urry, W. H. & Eiszner, J. R. The photochemical reactions of diazomethane with carbon tetrachloride and bromotrichloromethane. *J. Am. Chem. Soc.* **73**, 2977 (1951).
38. Chirpich, T. P., Zappia, V., Costilow, R. N. & Barker, H. A. Lysine 2, 3-aminomutase: purification and properties of a pyridoxal phosphate and S-adenosylmethionine-activated enzyme. *J. Biol. Chem.* **245**, 1778–1789 (1970).
39. Han, O. & Frey, P. A. Chemical model for the pyridoxal 5′-phosphate dependent lysine aminomutases. *J. Am. Chem. Soc.* **112**, 8982–8983 (1990).
40. Ye, C.-X., Shen, X., Chen, S.-M. & Meggers, E. Stereocontrolled 1, 3-nitrogen migration to access chiral α-amino acids. *Nat. Chem.* **14**, 566–573 (2022).
41. Fan, W. et al. Biomimetic 1,2-amino migration via photoredox catalysis. *Nat. Chem.* **17**, 941–951 (2025).
42. Wei, D. et al. Radical 1, 4/5-amino shift enables access to fluoroalkyl-containing primary β (γ)-aminoketones under metal-free conditions. *Angew. Chem. Int. Ed.* **60**, 26308–26313 (2021).
43. Li, Y. et al. A copper-catalyzed aerobic [1,3]-nitrogen shift through nitrogen-radical 4-exo-trig cyclization. *Angew. Chem. Int. Ed.* **56**, 15436–15440 (2017).
44. Zhao, M.-N., Zhang, Z.-J., Ren, Z.-H., Yang, D.-S. & Guan, Z.-H. Copper-catalyzed oxidative cyclization/1, 2-amino migration cascade reaction. *Org. Lett.* **20**, 3088–3091 (2018).
45. Egami, H., Kawamura, S., Miyazaki, A. & Sodeoka, M. Trifluoromethylation reactions for the synthesis of β-trifluoromethylamines. *Angew. Chem. Int. Ed.* **52**, 7841–7844 (2013).
46. Liu, J. et al. Nickel-catalyzed radical Heck-type $C(sp^3)$–$C(sp^2)$ coupling cascades enabled by bromoalkane-directed 1,4-aryl shift: access to olefinated arylalanines. *Org. Lett.* **24**, 8192–8196 (2022).
47. Hong, Y. et al. Radical 1, 2-nitrogen migration cascades of β-bromo α-amino acid esters to access β-amino acid motifs enabled by cooperative Ni/Diboron catalysis. *Acs. Catal.* **14**, 5491–5502 (2024).
48. Zhao, G.-Y. et al. Nickel-catalyzed radical migratory coupling enables C-2 arylation of carbohydrates. *J. Am. Chem. Soc.* **143**, 8590–8596 (2021).
49. Wang, H., Han, W., Noble, A. & Aggarwal, V. K. Dual Nickel/Photoredox-catalyzed site-selective cross-coupling of 1, 2-bis-boronic esters enabled by 1, 2-boron shifts. *Angew. Chem. Int. Ed.* **61**, e202207988 (2022).
50. DeLano, T. J. et al. Nickel-catalyzed asymmetric reductive cross-coupling of α-chloroesters with (hetero) aryl iodides. *Chem. Sci.* **12**, 7758–7762 (2021).
51. Guan, H.-X., Zhang, Q.-W., Walsh, P. J. & Mao, J.-Y. Nickel/photoredox-catalyzed asymmetric reductive cross-coupling of racemic α-chloro esters with aryl iodides. *Angew. Chem. Int. Ed.* **59**, 5172–5177 (2020).
52. Tang, S. et al. Visible-light-induced perfluoroalkylation/arylmigration/desulfonylation cascades of conjugated tosyl amides. *Tetrahedron Lett.* **58**, 329–332 (2017).
53. Chen, D.-F., Han, Z.-Y., Zhou, X.-L. & Gong, L.-Z. Asymmetric organocatalysis combined with metal catalysis: concept, proof of concept, and beyond. *Acc. Chem. Res.* **47**, 2365–2377 (2014).
54. Du, Z.-T. & Shao, Z.-H. Combining transition metal catalysis and organocatalysis–an update. *Chem. Soc. Rev.* **42**, 1337–1378 (2013).
55. Chen, D.-F. & Gong, L.-Z. Organo/transition-metal combined catalysis rejuvenates both in asymmetric synthesis. *J. Am. Chem. Soc.* **144**, 2415–2437 (2022).

56. Xu, X., Peng, L., Chang, X. & Guo, C. Ni/chiral sodium carboxylate dual catalyzed asymmetric O-propargylation. *J. Am. Chem. Soc.* **143**, 21048–21055 (2021).
57. Lelais, G. & Seebach, D. β^2-amino acids-syntheses, occurrence in natural products, and components of β-peptides. *J. Pept. Sci.* **76**, 206–243 (2004).
58. Seebach, D. & Gardiner, J. β-Peptidic peptidomimetics. *Acc. Chem. Res.* **41**, 1366–1375 (2008).
59. Cheng, J.-S., Qi, X.-X., Li, M., Chen, P.-H. & Liu, G.-S. Palladium-catalyzed intermolecular aminocarbonylation of alkenes: efficient access of β-amino acid derivatives. *J. Am. Chem. Soc.* **137**, 2480–2483 (2015).
60. Davies, J. et al. Ni-catalyzed carboxylation of aziridines en route to β-amino acids. *J. Am. Chem. Soc.* **143**, 4949–4954 (2021).
61. Tan, G.-Y. et al. Photochemical single-step synthesis of β-amino acid derivatives from alkenes and (hetero) arenes. *Nat. Chem.* **14**, 1174–1184 (2022).
62. Davies, H. M. L. & Venkataramani, C. Catalytic enantioselective synthesis of β^2-amino acids. *Angew. Chem. Int. Ed.* **41**, 2197–2199 (2002).
63. Zhu, C., Mandrelli, F., Zhou, H., Maji, R. & List, B. Catalytic asymmetric synthesis of unprotected β^2-amino acids. *J. Am. Chem. Soc.* **143**, 3312–3317 (2021).
64. Zhang, D. et al. Development of β-amino acid dehydrogenase for the synthesis of β-amino acids via reductive amination of β-keto acids. *ACS Catal.* **5**, 2220–2224 (2015).
65. Blake, J. F. et al. Discovery and Preclinical Pharmacology of a Selective ATP-Competitive Akt Inhibitor (GDC-0068) for the Treatment of Human Tumors. *J. Med. Chem.* **55**, 8110–8127 (2012).
66. Tang, S. et al. Radical 1,4-aryl migration enabled remote cross-electrophile coupling of α-amino-β-bromo acid esters with aryl bromides. *Angew. Chem. Int. Ed.* **60**, 21360–21367 (2021).
67. Liu, Y.-L. et al. A radical 1,4-aryl migration enables nickel catalysed remote cross-electrophile coupling of β-bromo amino acid esters with vinyl triflates. *Chem. Commun.* **60**, 4306–4309 (2024).
68. Xu, H., Zhao, C., Qian, Q., Deng, W. & Gong, H. Nickel-catalyzed cross-coupling of unactivated alkyl halides using bis(pinacolato) diboron as reductant. *Chem. Sci.* **4**, 4022–4029 (2013).
69. Sheng, J. et al. Diversity-oriented synthesis of aliphatic fluorides via reductive $C(sp^3)$–$C(sp^3)$ cross-coupling fluoroalkylation. *Angew. Chem. Int. Ed.* **60**, 15020–15027 (2021).
70. Sun, D.-L., Gong, Y.-X., Wu, Y., Chen, Y.-R. & Gong, H.-G. Optimal electrocatalyst design strategies for acidic oxygen evolution. *Adv. Sci.* **11**, 2198–3844 (2024).
71. Xu, M.-M. et al. Enantioselective cross-[4+2]-cycloaddition/decarboxylation of 2-pyrones by cooperative catalysis of the Pd(0)/NHC complex and chiral phosphoric acid. *J. Am. Chem. Soc.* **146**, 6936–6946 (2024).
72. Tao, Z.-L., Zhang, W.-Q., Chen, D.-F., Adele, A. & Gong, L.-Z. Pd-catalyzed asymmetric allylic alkylation of pyrazol-5-ones with allylic alcohols: the role of the chiral phosphoric acid in C–O bond cleavage and stereocontrol. *J. Am. Chem. Soc.* **135**, 9255–9258 (2013).
73. Li, G., Ji, C.-L., Hong, X. & Szostak, M. Highly chemoselective, transition-metal-free transamidation of unactivated amides and direct amidation of alkyl esters by N–C/O–C cleavage. *J. Am. Chem. Soc.* **141**, 11161–11172 (2019).
74. Liu, W.-B., Li, L. & Li, C.-J. Empowering a transition-metal–free coupling between alkyne and alkyl iodide with light in water. *Nat. Commun.* **6**, 6526 (2015).
75. Woods, B. P., Orlandi, M., Huang, C., Sigman, M. S. & Doyle, A. G. Nickel-catalyzed enantioselective reductive cross-coupling of styrenyl aziridines. *J. Am. Chem. Soc.* **139**, 5688–5691 (2017). 16.
76. Pietsch, S. et al. Synthesis, structure, and reactivity of anionic sp^2–sp^3 diboron compounds: readily accessible boryl nucleophiles. *Chem. Eur. J.* **21**, 7082–7098 (2015).
77. Dang L., Lin, Z. & Marder, T. B. Boryl ligands and their roles in metal-catalysed borylation reactions. *Chem. Commun.* **27**, 3987–3995 (2009).
78. Biswas, S. & Weix, D. J. Mechanism and selectivity in nickel-catalyzed cross-electrophile coupling of aryl halides with alkyl halides. *J. Am. Chem. Soc.* **135**, 16192–16197 (2013).
79. Zhang, Y. et al. Catalytic cross-electrophile coupling of aryl chlorides with unactivated alkyl chlorides: the synergy of iron and Li. *Chem* **9**, 3623–3636 (2023).
80. Li, M.-B., Wang, Y. & Tian, S.-K. Regioselective and stereospecific cross-coupling of primary allylic amines with boronic acids and boronates through palladium-catalyzed C-N bond cleavage. *Angew. Chem. Int. Ed.* **51**, 2968–2971 (2012).
81. Jacob, J. A., Garwood, J. J. A., Chen, A. D. & Nagib, D. V. Radical polarity. *J. Am. Chem. Soc.* **146**, 28034–28059 (2024).
82. Merritt, J. M. et al. Hydrogen evolution from telescoped Miyaura borylation and Suzuki couplings utilizing diboron reagents: process safety and hazard considerations. *Org. Process Res. Dev.* **26**, 773–784 (2022).
83. Becke, A. D. A new mixing of Hartree–Fock and local density-functional theories. *J. Chem. Phys.* **98**, 1372 (1993).
84. Siegbahn, P. E. M., Blomberg, M. R. A. & Chen, S.-L. Significant van der Waals effects in transition metal complexes. *J. Chem. Theory Comput.* **6**, 2040–2044 (2010).
85. Goerigk, L. & Grimme, S. A thorough benchmark of density functional methods for general main group thermochemistry, kinetics, and noncovalent interactions. *Phys. Chem. Chem. Phys.* **13**, 6670–6688 (2011).

Acknowledgements

We are grateful for financial support from National Natural Science Foundation of China (Nos. 22271118 (S.T.) and 22173007 (S.C.)).

Author contributions

S.T. conceived the idea and directed the project.. Z.-C.L., Z.-J.L., M.X., L.Z., G.D., and X.L. performed the nickel-catalyzed synthesis and designed the substrate scope. Z.-C.L. and Y.D. performed the chiral HLPC analysis. S.C. and Z.M. performed the density functional calculations. S.T., J.L., and S.W. wrote the manuscript and contributed to data analysis and scientific discussion.

Competing interests

The authors declare no competing interests.

Additional information

Supplementary information The online version contains supplementary material available at https://doi.org/10.1038/s41467-025-62092-3.

Correspondence and requests for materials should be addressed to Shilu Chen, Jinheng Li or Shi Tang.

Peer review information *Nature Communications* thanks Junfeng Yang and the other anonymous reviewer(s) for their contribution to the peer review of this work. A peer review file is available.